

## Article

# Metabolomic and Transcriptomic Analyses Reveal Association of Mature Fruit Pericarp Color Variation with Chlorophyll and Flavonoid Biosynthesis in Wax Gourd (*Benincasa hispida*)

Jinqiang Yan <sup>1,2</sup>, Piaoyun Sun <sup>1,2</sup>, Wenrui Liu <sup>1,2</sup>, Dasen Xie <sup>1,2</sup>, Min Wang <sup>1,2</sup>, Qingwu Peng <sup>1</sup>, Qingming Sun <sup>3,\*</sup> and Biao Jiang <sup>1,2,\*</sup>

<sup>1</sup> Vegetable Research Institute, Guangdong Academy of Agricultural Sciences, Guangzhou 510640, China

<sup>2</sup> Guangdong Key Laboratory for New Technology Research of Vegetables, Guangzhou 510640, China

<sup>3</sup> Institute of Fruit Tree Research, Guangdong Academy of Agricultural Sciences, Guangzhou 510640, China

\* Correspondence: qingmingsun@126.com (Q.S.); jiangbiao@gdaas.cn (B.J.)

**Abstract:** (1) Background: Wax gourd is an economically important vegetable crop in many tropical and sub-tropical countries in Asia. Fruit color is an important fruit quality trait, but the genetic, biochemical basis and regulatory network of fruit color variation in wax gourd are rarely studied. (2) Methods: In this study, two wax gourd inbred lines with different pericarp colors were used as materials to conduct joint metabolomic and transcriptomic analyses on mature fruit pericarp: B214 with yellow and B227 with dark green color. (3) Results: It was found that the chlorophyll content in the pericarp of B214 was significantly lower than that of B227, consistent with the down-regulation of several genes involved in the chlorophyll biosynthesis pathway, including *hemA*, *hemB*, *hemC*, *hemF*, *chlH*, *chlI*, *chlM*, *POR*, and *CAO*. The 229 metabolites showed differential accumulation levels between B214 and B227, and 4 anthocyanins, 5 flavanones, 25 flavones, 25 flavone C-glycosides, 12 flavonols, and 3 isoflavones were identified. In particular, cyanidin 3-O-glucoside, an anthocyanin contributing to the coloration of dark color, showed higher accumulation in B227 than in B214, probably due to the higher expression of genes of *F3'H* and *glucosyl transferases (GTs)* in B227. Transcription factors such as MYBs and bHLHs showed differential expressions between the two lines including *bHLH14*, a homolog of Arabidopsis *AtbHLH14* that had significantly higher expression in B227 than in B214. *bHLH14* was located in a region where the *pericarp color (pc)* locus was mapped, suggesting it may be a candidate gene for the *pc* locus. (4) Conclusions: This work supports the association of chlorophyll and flavonoid synthesis in wax gourd fruit color variation and also provides a good foundation for understanding the regulatory network for wax gourd coloration.



**Citation:** Yan, J.; Sun, P.; Liu, W.; Xie, D.; Wang, M.; Peng, Q.; Sun, Q.; Jiang, B. Metabolomic and Transcriptomic Analyses Reveal Association of Mature Fruit Pericarp Color Variation with Chlorophyll and Flavonoid Biosynthesis in Wax Gourd (*Benincasa hispida*). *Agronomy* **2022**, *12*, 2045. <https://doi.org/10.3390/agronomy12092045>

Academic Editor: Antonio Lupini

Received: 29 July 2022

Accepted: 25 August 2022

Published: 27 August 2022

**Publisher's Note:** MDPI stays neutral with regard to jurisdictional claims in published maps and institutional affiliations.



**Copyright:** © 2022 by the authors. Licensee MDPI, Basel, Switzerland. This article is an open access article distributed under the terms and conditions of the Creative Commons Attribution (CC BY) license (<https://creativecommons.org/licenses/by/4.0/>).

**Keywords:** wax gourd; pericarp color; metabolomics; transcriptomic; *bHLH14*

## 1. Introduction

Wax gourd (*Benincasa hispida* (Thunb.) Cogn,  $2n = 2x = 24$ ) is an economically important vegetable crop widely cultivated in many tropical and sub-tropical countries in Asia [1]. The very large fruit of wax gourd is characterized by having a long shelf life, and may be stored for over five months, making it ideal for off-season consumption. In addition, it is also considered to have medicinal value in treating diseases, such as peptic ulcers, hemorrhages from internal organs, and epilepsy as well as other neurological disorders [2].

Like many other cucurbits such as cucumber, melon, watermelon, and pumpkin/squash, the fruit color of wax gourd is an important fruit quality trait affecting consumers' acceptance/preference. The colors of most flowers, fruits, and seeds are imparted by endogenous pigments including anthocyanins, flavonols, flavones, chlorophyll, and carotenoid [3,4]. For instance, in cucumber, green fruits contain higher chlorophyll content in the pericarp and more chloroplasts in the epidermis than white ones [5,6]. The biosynthetic pathways for flavonoids and chlorophyll have been extensively studied. Synthesis of colorless

and colorful flavonoids is initiated from three malonyl-CoA and one 4-coumaroyl-CoA molecules. The enzymes involved include chalcone synthase (CHS), chalcone isomerase (CHI), flavonoid 3-hydroxylase (F3H), flavonoid 3'-hydroxylase (F3'H), dihydroflavonol reductase (DFR), flavonol synthase (FLS), leucoanthocyanidin oxidase (LDOX), and UDP-glucose: flavonoid 3-O-glucosyl transferase (UFGT). FLS catalyzes the production of colorless flavonoids [7] such as leucocyanidin, leucopelargonidin, and leucodelphinidin, which are further catalyzed by LDOX to cyanidin, pelargonidin, and delphinidin, respectively. The colorless cyanidin, pelargonidin, and delphinidin are glycosylated by UFGT to the stable colorful anthocyanins [8]. Genes for the enzymes in the flavonoid pathways have also been well characterized. The chlorophyll pathway starts from glutamic acid, and involves many genes, including *hemA*, *hemB*, *hemC*, *chlI*, *POR*, and *PAO*, in the synthetic process.

In addition to the genes involved in the flavonoid and chlorophyll synthesis pathways, many transcription factors (TFs), especially the MYB class of TFs, have been shown to play important roles in regulating fruit color formation in plants. For example, apple *MdMYB1* is a core transcriptional regulator of the anthocyanin pathway; up-regulation of *MdMYB1* correlates with increased anthocyanin biosynthesis and the formation of red skin [9,10]. The expression level of *MYB7* in kiwifruit is correlated with carotenoid and chlorophyll pigment contents by activating genes in their synthetic pathways [11]. *PavMYB10.1* and *PyMYB114* regulate anthocyanin synthesis and affect the fruit color of sweet cherry and pear, respectively [12,13]. The basic Helix-Loop-Helix (bHLH) TFs have also been characterized as having vital roles in coloration. For example, in *Brassica rapa*, a large insertion in a bHLH TF gene *BrTT8* results in seed color change from black to yellow by controlling the expression of biosynthetic genes in the flavonoid pathway [14]. Other TF genes such as in the production of *Anthocyanin Pigment 1 (PAP1)* [15,16] and *Transparent Testa 2 (TT2)* [17] are also involved in the regulation of the flavonoid pathway. In addition to classical map-based cloning, new omic techniques such as metabolic and transcriptomic analyses have greatly improved our ability to understand the complex regulatory networks that control plant organ coloration [18,19]. Based on comparative transcriptomic analysis, it has been found that the chlorophyll biosynthesis process plays an important role in differentiating between the yellow and green stigma color of melon [20]. Based on the metabolomic and transcriptomic analyses of bitter and non-bitter genotypes of *Luffa*, researchers have found that the enriched genes in the cucurbitacin biosynthesis pathway may lead to the accumulation of metabolites such as isocucurbitacin B, cucurbitacin D, 23,24-dihydro cucurbitacin E, and cucurbitacin F, thus leading to the bitterness of *Luffa* [21]. A comprehensive floral transcriptomic comparison between a male fertile line and its near-isogenic male sterile line illustrated that genes may be associated with male sterility in watermelon [22], and subsequently verified that eight genes are responsible for watermelon male fertility via virus-induced gene silencing [23].

The skin color of wax gourd fruit varies from yellow, light green, and green to dark green. Using segregating populations derived from the cross between wax gourd inbred lines B214 (yellow pericarp) and B227 (dark green pericarp), we recently reported the inheritance of wax gourd skin color, which is controlled by a single locus *pc*, with dark green being dominant to yellow [24].

In order to further understand the chemical components and gene regulatory network involved in the regulation of coloration in wax gourd, integrated transcriptomic and metabolomic analyses were performed using two inbred lines with distinct pericarp colors. The results will provide valuable information for understanding the complex mechanism of the coloration of wax gourd and its breeding applications.

## 2. Materials and Methods

### 2.1. Plant Materials

Two wax gourd inbred lines, 'B214' and 'B227', were used as experimental materials in this study. 'B214' was an inbred line derived from a Taiwan landrace, and was with yellow-white skinned cylindrical fruit (longitudinal diameter 31 cm, diameter 12.8 cm), weighing

around 2.85 kg per fruit. ‘B227’ was an inbred line derived from a cultivar ‘Sanshui Heipi Donggua’, and was with dark green skinned long cylindrical fruit (longitudinal diameter 68 cm, diameter 21.8 cm), weighing around 14 kg per fruit (Figure 1). The two lines were grown in a test field at the Vegetable Research Institute, Guangdong Academy of Agricultural Sciences according to standard cultivation practices. One fruit was allowed to set on each plant. At 30 days after pollination, pericarp tissue from each mature fruit was collected with a razor blade, frozen in liquid nitrogen immediately, and kept at  $-80\text{ }^{\circ}\text{C}$  for further use.

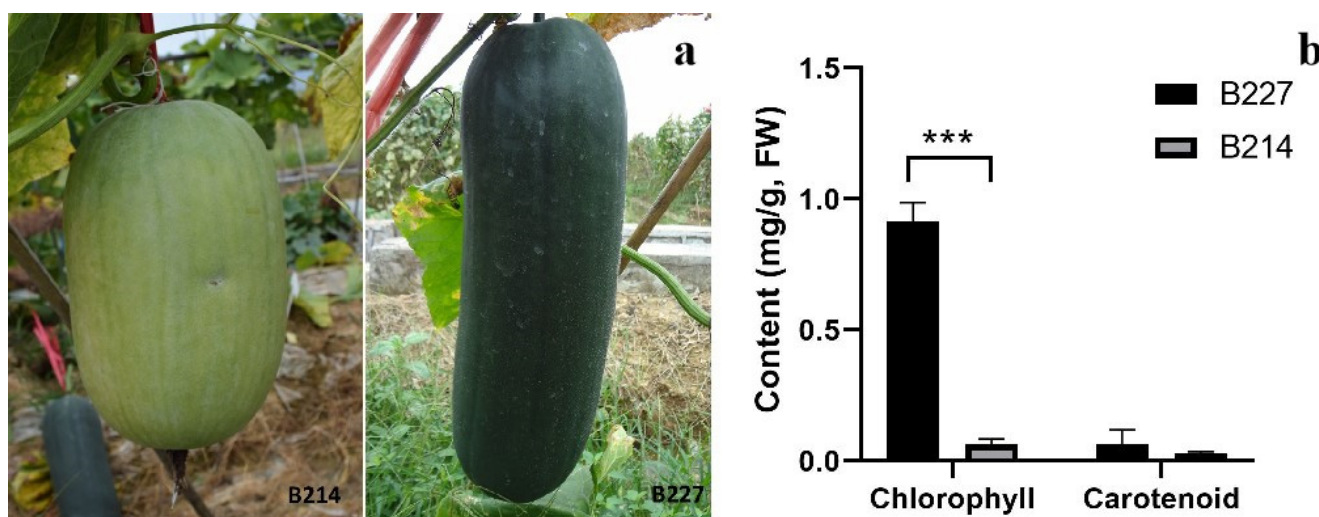


**Figure 1.** Phenotypic differences between mature fruit of B214 and B227: (a) Images of mature fruit of B214 (left) and B227 (right). (b) Chlorophyll and carotenoid content of mature pericarp of B214 and B227. FW, fresh weight. \*\*\*,  $p < 0.001$ .

## 2.2. Measurement of Chlorophyll and Carotenoid Contents

To determine content of chlorophyll and carotenoids, 0.1 g tissue from each sample was cut into small pieces and put into 10 mL 80% (v/v) acetone and kept in dark until the tissue turned white. There were three technical replicates for each sample. The absorbance of each sample was measured at 645, 663, and 470 nm, respectively. The concentrations of chlorophyll and carotenoid were calculated as described before [25].

## 2.3. Metabolite Measurements and Data Analysis

Each pericarp sample was grounded into fine powder using a mix mill (MM 400, Retsch, Germany) with a zirconia bead for 1.5 min at 30 Hz. The powder (100 mg) was dissolved in 1 mL 70% methanol, which was kept at  $4\text{ }^{\circ}\text{C}$  overnight. After  $10,000\times g$  centrifugation for 10 min, the supernatant was passed through an SPE Cartridge (CNWBOND carbon-GCB, 250 mg, 3 mL ANPEL, Shanghai, China, [www.anpel.com.cn](http://www.anpel.com.cn), accessed on 9 October 2017) and filtered by microporous filtering film (SCAA-104,  $0.22\text{ }\mu\text{m}$  pore size, ANPEL, Shanghai, China). Metabolites in the samples were then analyzed using an Ultra Performance Liquid Chromatography–Tandem Mass Spectrometry (UPLC-MS/MS) system (UPLC, Shim-pack UFLC SHIMADZU CBM30A, <http://www.shimadzu.com.cn/>, accessed on 9 October 2017; MS, Applied Biosystems 4500 QTRAP, <http://www.appliedbiosystems.com.cn/>, accessed on 9 October 2017). The analytical conditions were as follows: chromatographic column: Waters ACQUITY UPLC HSS T3 C18,  $1.8\text{ }\mu\text{m}$ ,  $2.1\text{ mm} \times 100\text{ mm}$ ; binary solvent system: solvent A (ultra-pure water containing 0.04% acetic acid), solvent B (acetonitrile containing 0.04% acetic acid); elution gradient: 95:5 V(A)/V(B) at 0 min, 5:95 V(A)/V(B) at 11.0 min, 5:95 V(A)/V(B) at 12.0 min, 95:5 V(A)/V(B) at 12.1 min, 95:5 V(A)/V(B) at 15 min; flow rate: 0.40 mL/min; temperature:  $40\text{ }^{\circ}\text{C}$ , and injection volume: 5 mL. Subsequently, the UPLC effluent was connected to an electrospray ionization (ESI)-triple quadrupole-linear ion trap (QTRAP)-MS/MS system.

Metabolite qualification and quantification were performed as previously described [26]. In brief, qualitative analysis of primary and secondary metabolites was based on the self-compiled database MWDB (MetWare Biotechnology Co., Ltd., Wuhan, China), and public databases, such as MassBank (<http://www.massbank.jp/>, accessed on 26 February 2018), KNApSACk (<http://kanaya.naist.jp/KNApSACk/>, accessed on 26 February 2018), HMDB (<http://www.hmdb.ca/>, accessed on 26 February 2018), MoToDB (<http://www.ab.wur.nl/moto/>, accessed on 26 February 2018), and METLIN (<http://metlin.scripps.edu/index.php/>, accessed on 26 February 2018). Metabolites were quantified using multiple-reaction monitoring (HRM). Integration and correction of chromatographic peaks were performed for all metabolites of mass spectra using MutiQuant version 3.0.2 (AB SCIEX, Concord, ON, Canada) [27]. The peak area integrals presented the relative number of corresponding metabolites.

Metabolites have been used for hierarchical clustering analysis (HCA), principal component analysis (PCA), and partial least squares-discriminant analysis (PLS-DA) to investigate the variety-specific accumulation of metabolites [28]. The *p*-value and fold change were 0.05 and 2.0, respectively.

#### 2.4. Transcriptome Profiling through RNA-Seq

Total RNA was extracted from the pericarp tissue of wax gourd inbred lines 'B214' and 'B227', with three biological replicates for each line. Samples were isolated using the Trizol Kit (Promega, Madison, WI, USA) according to the manufacturer's instructions, and treated with RNase-free DNase I (TaKaRa, Kyoto, Japan) to remove residual DNA. The quality of isolated RNA was verified with 1% RNase-free agarose gel electrophoresis. RNA concentration was measured by a 2100 Bioanalyzer. cDNA was synthesized with a cDNA Synthesis Kit (TaKaRa, Kyoto, Japan). The cDNA libraries were constructed using the Genomic Sample Prep Kit (Illumina), which were then paired-end sequenced on the Illumina His-Seq 2500 platform following 150 bp paired-end protocol at Metware Biotechnology Co., Ltd. (Wuhan, China).

Raw resequencing reads were processed by removing reads with adapter sequences, unknown nucleotides (>5%), or poor quality. Differentially expressed genes were identified with DESeqGs [29]. To explore the expression levels of DEGs, reads per kilobase of exon model per million mapped reads (RPKM) were applied, and an upper quartile algorithm was chosen for data correction [30]. Genes with at least a 2-fold difference in expression and  $|\log_2 \text{Fold Change}| \geq 1$  were considered to be DEGs as determined with the R statistical programming environment (<http://www.r-project.org>, accessed on 22 March 2018). All of the DEGs were analyzed by GO (gene ontology) enrichment using GOseq (1.10.0) [31] and KEGG (Kyoto Encyclopedia of Genes and Genomes) enrichment using KOBAS software [30].

#### 2.5. Validation of Gene Expression Level with Real-Time Quantitative PCR (qPCR)

The expression patterns of 12 DEGs were validated by qPCR (information presented in Table S4). Gene *F-box* was used as an internal control for the normalization of gene expression. Total RNA was extracted using the same methods in RNA-Seq described above. Samples were similar to those of RNA-seq but from different individuals of two lines, each also having three biological replicates. cDNA synthesis was performed using TransScript RT/RI enzyme mix with gDNA Remover (TransGen Biotech, Beijing, China, AT311-03). qPCR was performed in a 20  $\mu$ l volume with SYBR Premix Ex Taq (Takara, Kyoto, China) on a Bio-Rad CFX Connect Real-Time PCR System (Singapore). The amplification program was initiated at 95 °C for 10 min, followed by 45 cycles of 95 °C for 10 s, and 60 °C for 30 s. Relative expression levels were calculated using the  $2^{-\Delta\Delta C_t}$  method, where  $\Delta\Delta C_t = (C_{t_{\text{target}}} - C_{t_{\text{F-box}}})_{\text{B227}} - (C_{t_{\text{target}}} - C_{t_{\text{F-box}}})_{\text{B214}}$ . Three independent technical replicates of each sample were applied for real-time PCR.

### 3. Results

#### 3.1. Phenotypic Differences between B214 and B227 in Pericarp Color

There were obvious visual differences in the pericarp color of the wax gourd inbred lines B214 and B227. B214 presented yellow from the onset of fruit until the mature stage while B227 presented dark green. The mature fruit of B214 and B227 were shown in Figure 1a. During the mature fruit stage, the content of chlorophyll and carotenoid of mature pericarp of two lines was determined. The chlorophyll content of B214 was only 0.06 mg/g (FW, fresh weight), which was significantly lower than that of B227, 0.92 mg/g (FW, fresh weight) (Figure 1b). No significant difference was found between the carotenoid content of mature pericarp of B214 and B227 (Figure 1b).

#### 3.2. Metabolic Differences between Mature Pericarp of B214 and B227

To identify biochemical compounds that determine the fruit color of wax gourd, metabolic profiling of mature pericarp of B214 and B227, each with three biological replicates, was carried out based on the LC-MS/MS method. A total of 229 differentially accumulated metabolites (DAMs) were identified (Table S1). Compared with B214, B227 had 105 more accumulated DAMs (Table S1). The top ten accumulated metabolites in B214 were Rosinidin O-hexoside (Anthocyanins), Chrysoeriol C-pentosyl-O-hexosyl-O-hexoside (Flavone C-glycosides), Hesperetin O-Glucuronic acid (Flavanone), 8-C-hexosyl-apigenin O-hexosyl-O-hexoside (Flavone C-glycosides), di-C,C-hexosyl-apigenin (Flavone C-glycosides), Luteolin 6-C-hexoside 8-C-hexosyl-O-hexoside (Flavone C-glycosides), DIM-BOA glucoside (others), Tricin 5-O-rutinoside (Flavone), Pelargonidin 3-O-malonylhexoside (Anthocyanins), and 8-C-hexosyl chrysoeriol O-hexoside (Flavone C-glycosides) (Figure 2b). In contrast, the top ten accumulated metabolites in B227 were Riboflavin (Vitamins), Tricin O-glycerol (Flavone), 4-Hydroxy-3,5-diisopropylbenzaldehyde (Benzoic acid derivatives), Chrysin 5-O-glucoside (Flavone), 4-Oxoretinol (Vitamins), MGMG (18:2) isomer2 (Lipids\_Glycerolipids), Pelargonidin (Anthocyanins), DGMG (18:2) isomer2 (Lipids\_Glycerolipids), MAG (18:3) isomer3 (Lipids\_Glycerolipids), and MAG (18:3) isomer5 (Lipids\_Glycerolipids) (Figure 2b).

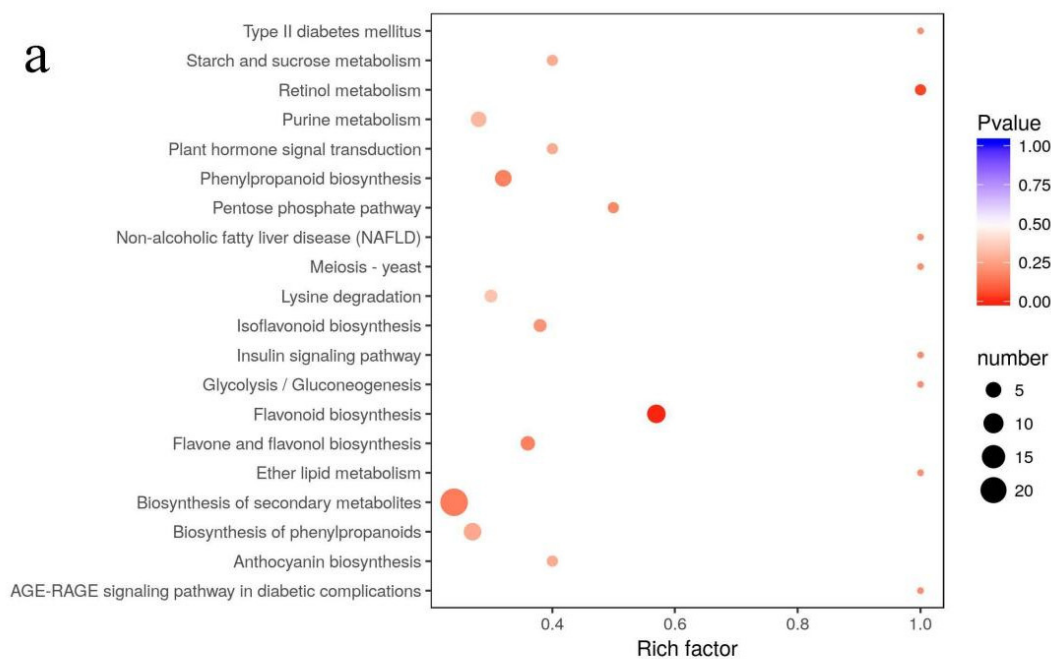
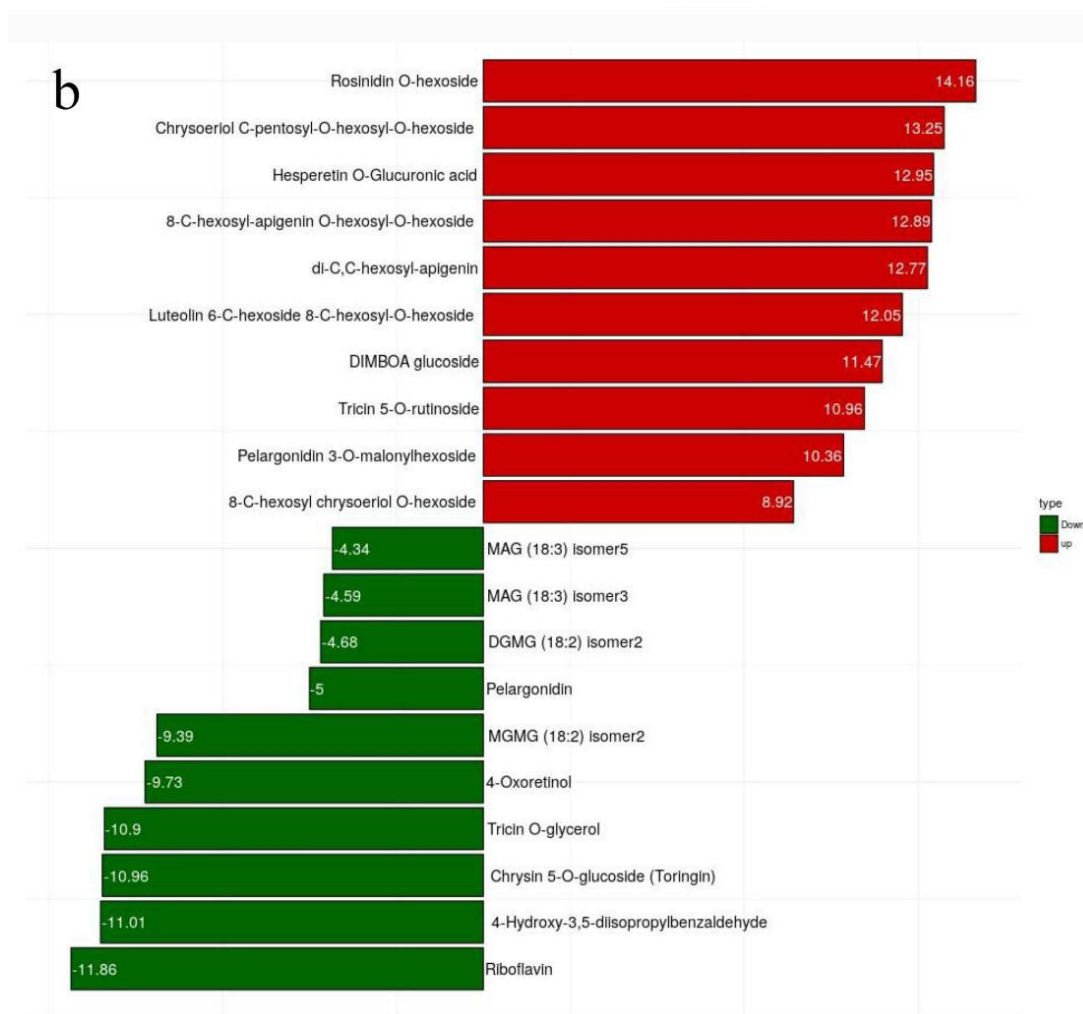


Figure 2. Cont.



**Figure 2.** Metabolome of mature pericarp of B214 and B227: (a) KEGG enrichment of DAMs in mature pericarp of B214 and B227. X-axis represents rich factor of each pathway and y-axis represents the names of pathways. Color of bubbles indicates the *p*-value, the redder, the more significant. Size of bubbles indicates the number of metabolites included in the pathway. (b) Representatives of 10 most up-accumulated and 10 most down-accumulated metabolites in B214. X-axis represents the value of Log2FoldChange (B214/B227) and y-axis represents the index of metabolites (Table S1).

The KEGG enrichment of 229 DAMs highlighted ‘Biosynthesis of secondary metabolites’ as the major pathway, distinguishing the two lines (Figure 2a). The ‘Phenylpropanoid biosynthesis’, ‘Flavonoid biosynthesis’, and ‘Purine biosynthesis’ pathways also showed obvious differences between the two lines (Figure 2a).

### 3.3. DAMs Associated with Flavonoid Biosynthesis Pathway

We further looked into DAMs in the flavonoid metabolic pathways. There were 4 anthocyanins, 5 flavanones, 25 flavones, 25 flavone C-glycosides, 12 flavonols, and 3 isoflavones (Table S1). The four anthocyanins were Rosinidin O-hexoside, Pelargonidin 3-O-malonylhexoside, Cyanidin 3-O-glucoside (Kuromanin), and Pelargonidin. The amounts of Cyanidin 3-O-glucoside (Kuromanin) and Pelargonidin were more concentrated in B227 than in B214, while the other two (Rosinidin O-hexoside and Pelargonidin 3-O-malonylhexoside) were detectable only in B214. However, 21 out of 25 flavone C-glycosides, except 4 (C-hexosyl-apigenin O-hexosyl-O-pentoside, C-hexosyl-apigenin O-pentoside, Apigenin 6-C-pentoside and C-hexosyl-apigenin C-pentoside), accumulated at higher levels in B214 than in B227 (Table S1).

### 3.4. Transcriptomic Analysis

From Illumina sequencing, 47,679,727 and 47,678,887 clean reads were obtained respectively from six B214 and B227 cDNA libraries (three replicates each; Table 1). The reads above Q20 for all libraries were above 97% (Table 1), indicating satisfactory sequencing quality. To compare differential expression between individuals, FPKM was used to denote transcript abundance. Based on FPKM values, the correlation coefficients among all samples were calculated in B214 and B227, which were all above 0.98 and 0.92, respectively (Figure 3a), indicating a high correlation among biological replicates. The DESeq2 was used to identify differentially expressed genes (DEGs) between the two samples. A DEG was defined as  $|\log_2\text{FoldChange}| \geq 1$  and false discovery rate (FDR)  $< 0.05$ . A total of 2576 DEGs were detected, of which 843 and 1724 were up- and down-regulated in dark-green fruited B227 as compared to light-colored B214 (Figure 3b; Table S2).

**Table 1.** Summary of RNA sequencing results after Illumina sequencing of B214 and B227.

Sample	Raw Reads	Clean Reads	Clean Base	Q20	Q30	GC Content
B214-1	48,005,504	47,722,880	7.12 G	97.96%	94.72%	43.89%
B214-2	47,993,264	47,625,966	7.11 G	97.68%	94.11%	43.85%
B214-3	47,999,846	47,690,334	7.11 G	97.88%	94.56%	44.11%
B227-1	48,009,350	47,703,118	7.12 G	97.89%	94.58%	44.09%
B227-2	47,976,656	47,650,708	7.11 G	97.85%	94.48%	44.25%
B227-3	47,984,830	47,682,834	7.12 G	97.91%	94.61%	44.55%

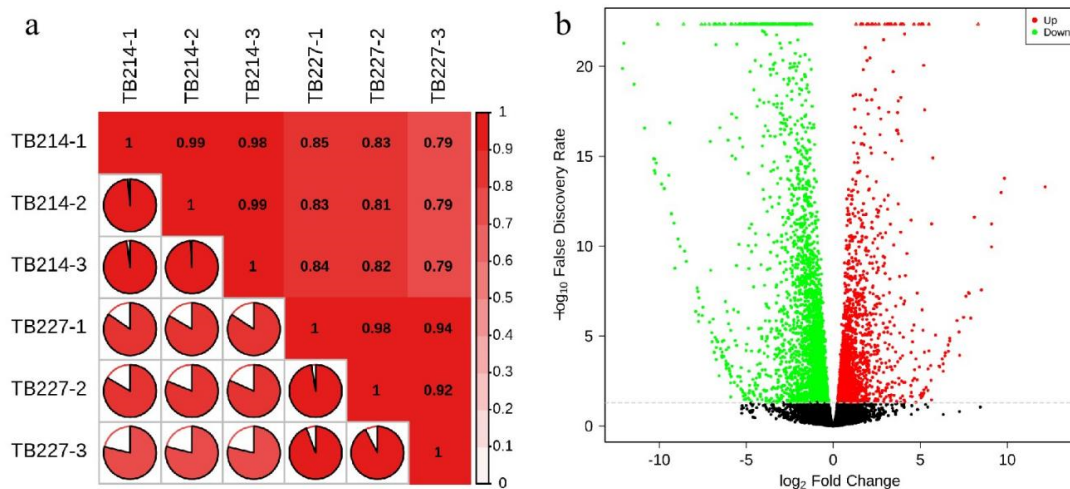


**Figure 3.** Statistical analysis of transcriptomic data of mature pericarps of B227 and B214: (a) Heatmap illustrating correlations between the two individual datasets based on  $R^2$ . Red color indicates a stronger correlation and white color indicates weak correlation. (b) Volcano plot showing DEGs between mature pericarp of B214 and B227. X-axis represents  $\log_2\text{FoldChange}$  (B214/B227) and y-axis represents  $-\log_{10}(p\text{-value})$ . Red and green dots indicate up-regulated and down-regulated genes, respectively. Black dots represent non-DEGs between B227 and B214.

### 3.5. Functional Classification of DEGs

GO and KEGG pathway enrichment analyses were performed to understand significantly enriched biological processes and pathways. As illustrated in Figure 4a, chloroplast related GO terms were enriched, including chloroplast thylakoid (GO:0009534,  $p = 2.78249 \times 10^{-35}$ ), chloroplast thylakoid membrane (GO:0009535,  $p = 7.68223 \times 10^{-29}$ ), chloroplast envelope (GO:0009941,  $p = 2.64615 \times 10^{-12}$ ), and chloroplast thylakoid lumen (GO:0009543,  $p = 4.76506 \times 10^{-10}$ ). Go terms related to photosynthesis and photosystem were also enriched (Figure 4a). In these GO terms, compared with B227, the expression of almost all genes in the mature pericarp of B214 was down-regulated.

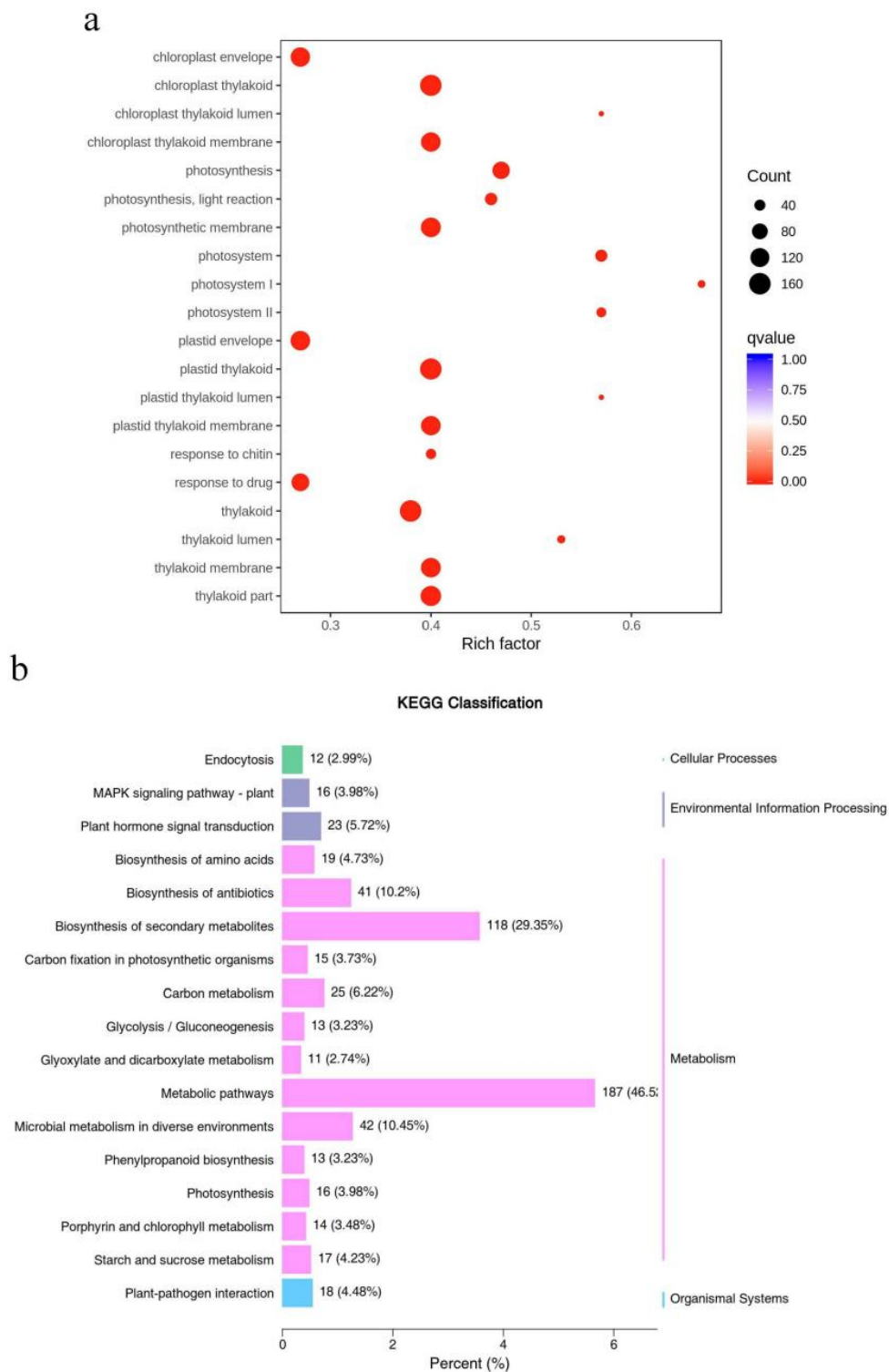


**Figure 4.** Functional classification of DEGs between pericarp of B214 and B227 mature fruit: (a) Enriched GO items. X-axis represents rich factor, which is the ratio between number of DEGs and number of genes assigned to the GO item. A big rich factor indicated a high enrichment level. Color of bubbles represents the *p* value, the redder, the more significant. Size of bubbles represents the number of DEGs in the item, the larger, the more quantities. Y-axis represents GO terms. (b) Histogram showing enriched KEGG pathways. X-axis represents the percentage of annotated genes in the pathway among all annotated genes. Y-axis represents the names of KEGG pathways. Categories of KEGG pathways were listed at the right side of the figure.

For KEGG classification, the DEGs were classified into four categories, i.e., “Cellular Processes”, “Environmental Information Process”, “Metabolism”, and “Organismal Systems” (Figure 4b). Most of the genes were assigned to “metabolism”. The “metabolic pathways” (ko\_id: ko01100,  $p = 0.0003319$ ) was the most enriched pathway in the category, with 46.52% of genes included (Figure 4b). “Photosynthesis” (ko\_id: ko00195,  $p = 9.07794 \times 10^{-8}$ ) and “Porphyrin and chlorophyll metabolism” (ko\_id: ko00860,  $p = 9.91039 \times 10^{-7}$ ) were also found enriched in “metabolism” category (Figure 4b).

### 3.6. DEGs Associated with Chlorophyll Biosynthesis Pathway

Porphyrin, and chlorophyll, metabolism were the pathways that were significantly enriched in KEGG analysis, and fourteen genes in KEGG were found to have different transcript abundance between B214 and B227 (Table S3). Since chlorophyll contents in the mature pericarp of B214 and B227 were significantly different, DEGs in the chlorophyll synthetic pathway were therefore examined. Many genes in this pathway were down-regulated in B214 (Table S2; Figure 5a,b), such as *hemA* (glutamyl-tRNA reductase, ID: evm.TU.Contig40.5), *hemB* (porphobilinogen synthase, ID: evm.TU.Contig799.3), *hemC* (hydroxymethylbilane synthase, ID: evm.TU.Contig265.18), *hemF* (coproporphyrinogen III oxidase, ID: evm.TU.Contig102.84), *chlH* (magnesium chelatase subunit H, ID: evm.TU.Contig579.8), *chlI* (magnesium chelatase subunit I, ID: evm.TU.Contig235.160), *chlM* (magnesium-protoporphyrin O-methyltransferase, ID: evm.TU.Contig0.4), *POR* (prochlorophyllide reductase, ID: evm.TU.Contig218.49), and *CAO* (chlorophyllide a oxygenase, ID: evm.TU.Contig57.63) (Figure 5a,b). Among them, the expression of *POR* in B227 was 4.533-fold higher than that in B214 (Table S2; Figure 5b).

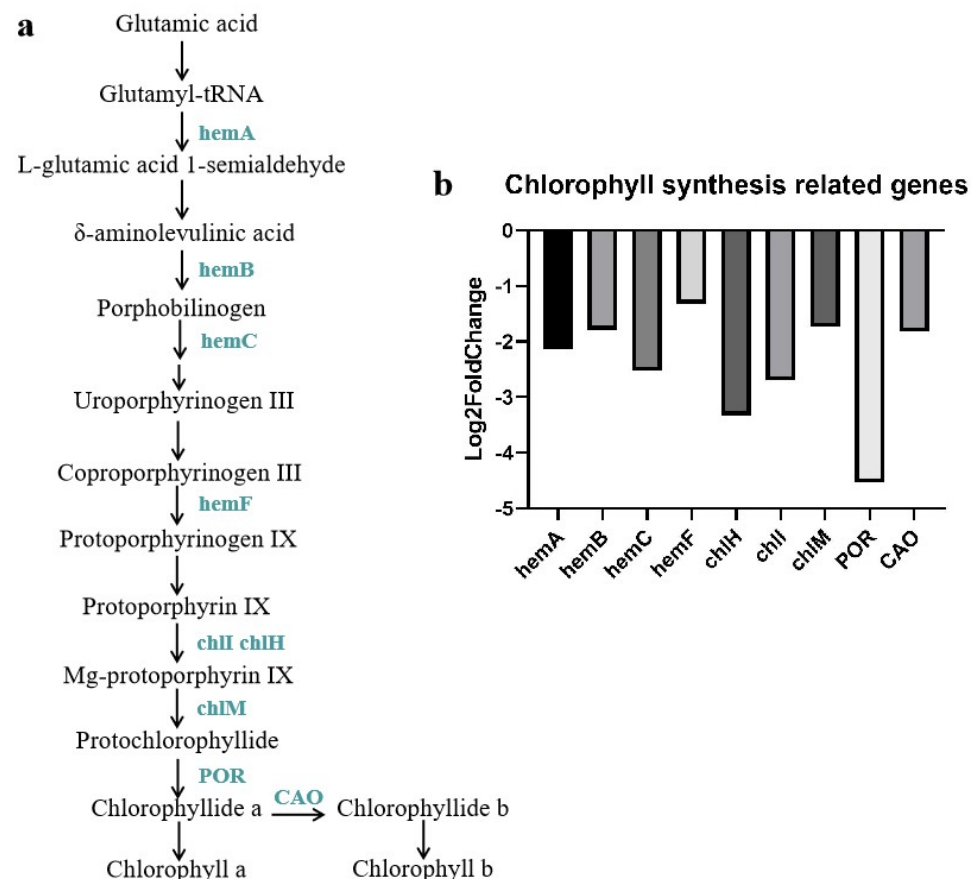


**Figure 5.** DEGs in chlorophyll synthetic pathway. (a) Flowchart showing chlorophyll synthetic pathway: Genes in blue indicated a down-regulation in B214. (b) Gene expression ratio B214/B227 represented using Log2FoldChange. X-axis represents the names of genes and y-axis represents the value of Log2FoldChange.

### 3.7. DEGs Associated with Photosynthesis

There is a close link between chlorophyll content and photosynthesis capacity in fruit [32]. Therefore, the expression of photosynthesis-related genes in the pericarp transcriptomes of the two lines was examined. All light-harvesting chlorophyll a/b-binding protein genes were significantly down-regulated in mature pericarp of B214 (Table 2) including *LHCA1*, *LHCA3*, *LHCB1*, *LHCB2*, *LHCB3*, *LHCB5*, and *LHCB6*. The expression of *LHCB6* in B227 was almost 10-fold of that in B214, which was confirmed in qRT-PCR (Figure 6).

**Table 2.** DEGs related to photosynthesis in the mature pericarp of B227 and B214.

ID	Gene	B227	B214	log2 Fold Change	p-Value	Regulated
evm.TU.Contig37.39	<i>LHCA3</i>	15,775	1488	−3.406	$9.18262 \times 10^{-27}$	down
evm.TU.Contig644.1	<i>LHCB1</i>	49,230	46	−10.084	$2.07354 \times 10^{-254}$	down
evm.TU.Contig224.65	<i>LHCB2</i>	54	8	−2.835	$4.07974 \times 10^{-8}$	down
evm.TU.Contig377.7	<i>LHCB3</i>	4102	6	−9.444	$2.51075 \times 10^{-16}$	down
evm.TU.Contig169.75	<i>LHCB5</i>	25,570	340	−6.232	$2.32559 \times 10^{-101}$	down
evm.TU.Contig512.42	<i>LHCB6</i>	7911	184	−5.43	$4.79903 \times 10^{-47}$	down

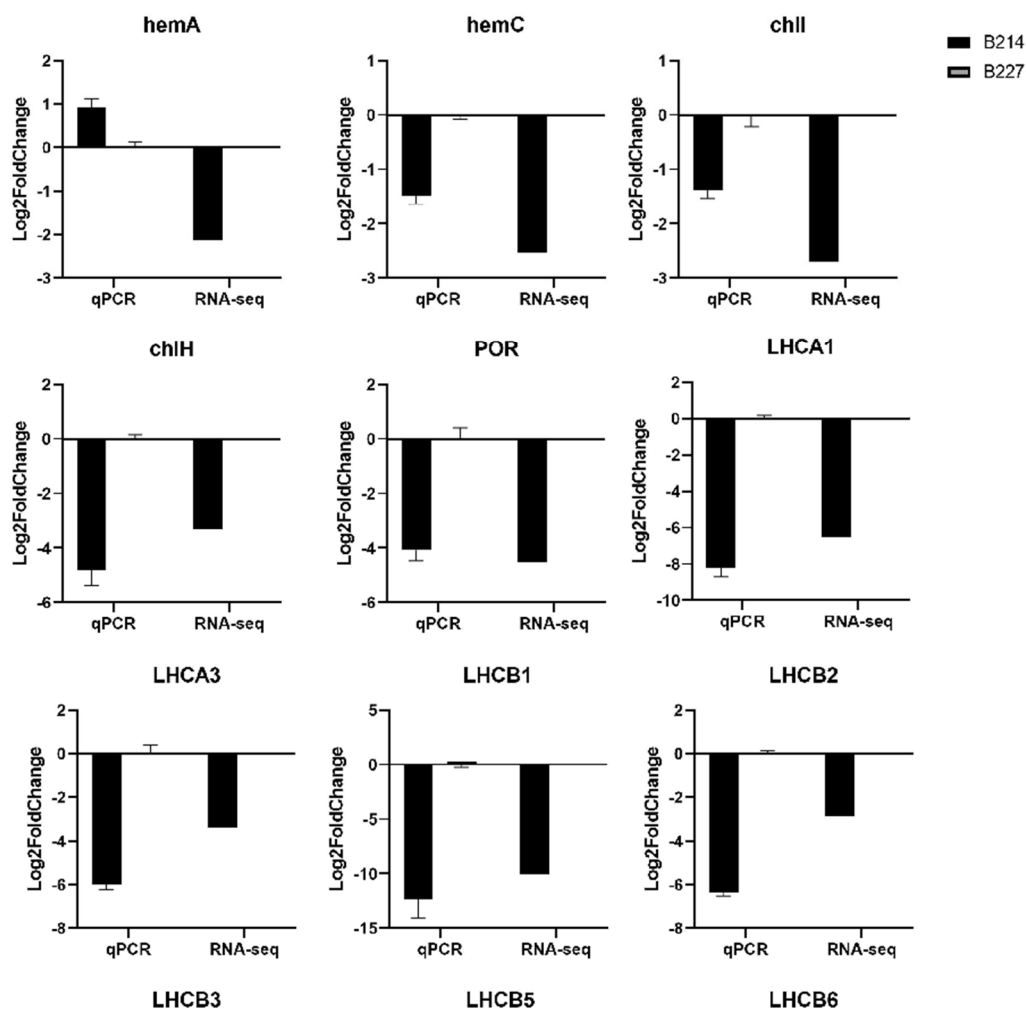


**Figure 6.** Cont.

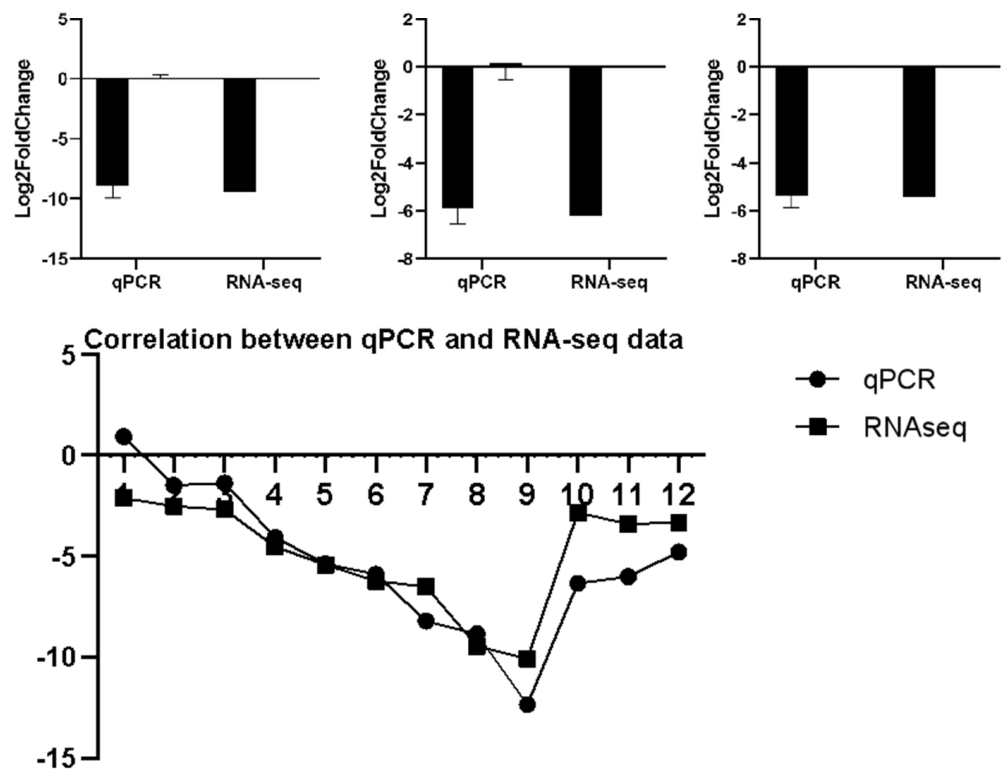


Figure 6. qRT-PCR verification of transcriptomic analysis results.

### 3.8. DEGs Associated with Flavonoid Biosynthesis Pathway

We examined expression patterns in the two lines that play roles in the flavonoid synthetic pathway such as *CHS*, *FLS*, *ANR*, *F3'5'H*, and *F3'H* (Table 3). All except *CHS* were down-regulated in B214. Both *F3'H* (ID: evm.TU.Contig87.40) and *F3'5'H* (ID: evm.TU.Contig87.39) were more abundant in B227, with a 4.149-fold and 1.782-fold increase, respectively. Synthesis of proanthocyanidins shared common steps with anthocyanin. *ANR* (Anthocyanidin reductase) promotes the production of proanthocyanidins rather than anthocyanin. *ANR* (ID: evm.TU.Contig705.13) showed a low expression level in the mature pericarp of B227 while no transcript was detected in B214. Three glucosyltransferases (*GT5* and *GT7s*) involved in the formation of anthocyanidins were found to have a relatively high transcript abundance in B227 (Table 2).

Table 3. DEGs involved in the flavonoid pathway in the mature pericarp of B227 and B214.

ID	Gene	B227	B214	log <sub>2</sub> Fold Change	p Value	Regulated
evm.TU.Contig115.34	<i>CHS</i>	442	936	1.081	$5.77 \times 10^{-8}$	up
evm.TU.Contig705.13	<i>ANR</i>	13	0	-6.141	$9.24 \times 10^{-5}$	down
evm.TU.Contig87.39	<i>F3'5'H</i>	311	90	-1.782	$4.42 \times 10^{-8}$	down
evm.TU.Contig87.40	<i>F3'H</i>	397	22	-4.149	$4.73 \times 10^{-11}$	down
evm.TU.Contig211.255	<i>FLS</i>	287	72	-1.989	0.000249	down
evm.TU.Contig416.27	<i>GT5</i>	37	10	-1.84	0.000831	down
evm.TU.Contig26.80	<i>GT7</i>	707	289	-1.292	$1.02 \times 10^{-5}$	down
evm.TU.Contig112.25	<i>GT7</i>	2966	1289	-1.203	0.000574	down

### 3.9. Expressions of bHLH and MYB Transcription Factors

TFs are important players in regulating flavonoid synthesis in horticultural crops. Among the DEGs, 189 were TFs including 14 bHLH and 27 MYB TFs (Table S2). Of the 14 bHLH DEGs, only *bHLH95* and *bHLH154* were up-regulated, while all the others were down-regulated in B214. *bHLH35* (ID: evm.TU.Contig391.9), a homolog of

*AtbHLH035*, was only expressed in B227. *bHLH14* was also found in with low abundance in B214 (Table 4). Among MYB DEGs, MYB-related protein 306 (ID: evm.TU.Contig10.51) had the most significant difference, homologous to AtMYB30, showing 8.115-fold increased expression in B214 than in B227. Among the down-regulated MYBs, AtMYB84 homolog (ID: evm.TU.Contig88.71) was not expressed in B214, but was slightly expressed in B227 (Table 5).

**Table 4.** Differentially expressed bHLHs in the mature pericarp of B214 and B227.

ID	Gene	B227	B214	log2 Fold Change	p Value	Regulated
evm.TU.Contig112.11	<i>bHLH95</i>	0	5	4.746	0.014	up
evm.TU.Contig164.13	<i>bHLH154</i>	8	290	5.197	$1.03 \times 10^{-22}$	up
evm.TU.Contig179.20	<i>bHLH14</i>	68	4	−4.1	$1.33 \times 10^{-6}$	down
evm.TU.Contig209.54	<i>bHLH14</i>	44	6	−2.968	0.0013	down
evm.TU.Contig234.152	<i>bHLH041</i>	11	1	−4.088	0.0095	down
evm.TU.Contig329.8	<i>bHLH92</i>	618	20	−4.968	$1.34 \times 10^{-36}$	down
evm.TU.Contig391.9	<i>bHLH35</i>	81	0	−8.801	$3.85 \times 10^{-12}$	down
evm.TU.Contig88.51	<i>bHLH25</i>	19	1	−4.295	0.0002	down

**Table 5.** Differentially expressed MYBs in the mature pericarp of B214 and B227.

ID	Gene	B227	B214	log2 Fold Change	p Value	Regulated
evm.TU.Contig10.51	<i>MYB30</i>	1	187	8.115	$7.25 \times 10^{-14}$	up
evm.TU.Contig105.117	<i>MYB14</i>	112	12	−3.218	$1.38 \times 10^{-11}$	down
evm.TU.Contig13.239	<i>MYB124</i>	2613	484	−2.434	$5.13 \times 10^{-19}$	down
evm.TU.Contig177.101	<i>MYB3</i>	22	734	5.105	$3.01 \times 10^{-65}$	up
evm.TU.Contig198.7	<i>MYB4</i>	3	17	2.312	0.004023	up
evm.TU.Contig216.35	<i>MYB38</i>	85	16	−2.45	$6.35 \times 10^{-9}$	down
evm.TU.Contig328.27	<i>MYB15</i>	11	1	−3.109	0.008564	down
evm.TU.Contig356.67	<i>MYB86</i>	128	541	2.079	$1.61 \times 10^{-15}$	up
evm.TU.Contig493.41	<i>MYB14</i>	41	6	−2.852	0.00111	down
evm.TU.Contig57.22	<i>MYB62</i>	21	1	−3.991	0.002206	down
evm.TU.Contig88.71	<i>MYB84</i>	6	0	−5.016	0.009042	down
evm.TU.Contig96.61	<i>MYB16</i>	3	96	4.824	$2.3 \times 10^{-9}$	up
evm.TU.Contig98.10	<i>MYB2</i>	182	20	−3.17	$1.13 \times 10^{-6}$	down

### 3.10. Real-Time PCR Validation of Transcriptomic Data

In order to confirm the reliability of transcriptomic results, qRT-PCR was performed to validate the key DEGs between B227 and B214 in chlorophyll synthetic and photosynthesis pathways. It could be seen that qPCR and RNA-seq data had a relatively similar expression trend among most of the verified genes (Figure 6). The qRT-PCR results were generally consistent with the RNA-Seq results (correlation coefficient = 0.8553). The real-time PCR verification confirmed the reliability of the transcriptomic analysis.

### 3.11. Combined Analysis of Transcriptome and Metabolome

DEGs and DAMs were simultaneously subjected to KEGG analysis to understand the pathways related to pericarp color variation in wax gourd. It could be seen that the ‘Flavone and flavonol biosynthesis’ pathway was the most significantly enriched KEGG pathway (Figure S1). In total, 3 DEGs and 50 DAMs were included in this pathway. The Pearson correlation coefficients between DEGs and DAMs were thereafter calculated. The correlation coefficient > 0.8 was considered significant. Each gene was correlated with more than one metabolite, and vice versa. The transcript *evm.TU.Contig251.2* encoding phenolic glucoside malonyltransferase 2, was correlated with the largest number of metabolites (35 out of 50 metabolites).

#### 4. Discussion

Mature fruits of cucurbit crops exhibit a wide range of color variations. Cucumber, for example, ranges in fruit color from white, light green, dark green, yellow, and orange to red [33]. In wax gourd, fruit color may range from yellow to dark green [24]. However, as far as we know, the underlying regulatory network of fruit color in wax gourd is still unknown. The purpose of this study is to unravel the regulatory network of wax gourd fruit color from the aspects of metabolism and transcriptome using two lines with distinct fruit colors, B214 with yellow and B227 with dark green, as examples.

Chlorophylls, carotenoids, and flavonoids are the main pigments underlying the diverse fruit colors in plants. In cucumber, the green fruit color directly correlates with the chlorophyll content in the pericarp [33]. In wax gourd, we also observed this correlation. A pericarp of dark green contained a high level of chlorophyll than a pericarp of yellow. However, no chlorophyll-related metabolites were detected, which was probably caused by the degradation of chlorophyll-related metabolites during the extraction process. From genetic aspects, many chlorophyll synthesis-related genes affecting fruit color have been reported. Variations in gene *CsYcf54* [34] and *APRR2* [5] disrupted normal chlorophyll synthesis, leading to light green and white cucumber fruit, respectively. *chlH*, a gene involved in chlorophyll synthesis pathway, is proposed as a strong candidate gene controlling fruit color in watermelon [35]. Transcriptomic analysis has also been applied to investigate molecular mechanisms either underlying leaf or fruit color differentiation. The change in the chlorophyll content in plant leaves has a strong correlation with the transcription level of genes in the chlorophyll synthesis pathway, such as *chlH*, *POR*, and *HEMA* [36,37]. Chlorophyll-related genes *HEMA*, *HEMB*, *CHLM*, and *POR* are down-regulated in cucumber with yellow-green fruit pericarp compared with that with dark green fruit pericarp [38]. In wax gourd, it was found that all detected DEGs in the chlorophyll synthesis pathway were down-regulated in yellow pericarp wax gourd. For example, the expression of *POR*, which catalyzes the conversion of protochlorophyllide into chlorophyllide a, was fourfold higher in a dark green pericarp wax gourd than in a yellow one. At the same time, we also examined the expression of chlorophyll degradation genes, *SGR* (*STAY-GREEN*, encoding Mg-dechelatase), *RCCR* (encoding red Chl catabolite reductase), *PAO* (encoding pheophorbide a oxygenase), and *PPH* (encoding pheophytinase), but no significant difference was found. Even in melon stigma, the expression of *POR*, *CAO*, and *chlH* also had a higher expression level in a green one than in a yellow one [20]. The results indicate that the chlorophyll content in wax gourd pericarp was more correlated with the expression of chlorophyll synthetic genes than chlorophyll degradation genes, and chlorophyll synthetic genes may play a general function in the formation of green color in different plant organs. It is therefore hypothesized that the high expression rate of chlorophyll-synthesis genes leads to a green pericarp in wax gourd.

Flavonoids are a large cluster of chemical compounds that impart many colors to flowers, leaves, and fruits [39–41]. Based on the combined transcriptome and metabolome analysis, the ‘Flavone and flavonol biosynthesis’ pathway was the most significantly enriched KEGG pathway. Most flavones had a higher concentration in B214 than in B227, which is consistent with the finding in melon where the content of flavones was higher in grey-green than in yellow-colored melon [42]. Cyanidin 3-O-glucoside promotes the coloration of dark colors such as purple and black [43,44], and *F3'H* is the most important enzyme for the synthesis of Cyanidin 3-O-glucoside [45,46]. An abundant expression level of *F3'H* is accompanied by a high accumulation of Cyanidin 3-O-glucoside in the dark green pericarp of wax gourd. 3-O-Glucosyltransferase (GTs) is the last step and a key step in the process of anthocyanin coloration from unstable to stable. In our transcriptomic data, all GTs were found to be highly expressed in fruits with deep color, consistent with other studies [47,48]. At the same time, it was found that nearly all flavone C-glycosides were more abundant in yellow pericarp than that in dark green. Previously, C-glycosides were reported as being responsible for the yellow coloration of bracts in *Zantedeschia Aethiopica* [49]. Therefore, we proposed that cyanidin 3-O-glucoside and

flavone C-glycosides may respectively serve as chemical indicators for the dark green and yellow pericarp color of wax gourd.

In most cases, coloration is regulated in a complex manner, with TF dominating other coloration-related genes. Here, we identified many *bHLH* and *MYB* DEGs between the two wax gourd lines including *bHLH14* (*evm.TU.Contig179.20*), a homolog of Arabidopsis *AtbHLH14*, with a higher expression in the mature pericarp of B227 than in B214. We compared the genomic DNA sequences of *bHLH14* between the two lines and found a 6 bp deletion in the exon of this gene in the yellow-colored B214. An indel marker based on the 6 bp deletion was co-segregating with the yellow/dark green pericarp color (*pc* locus) in populations derived from crosses between B214 and B227 (Jiang et al. unpublished data). In Arabidopsis, overexpression of *AtbHLH14* delays jasmonate (JA)-induced leaf senescence (yellow leaf, lower chlorophyll content) [50]. *AtbHLH14* has also been shown to play a role in JA-induced anthocyanin accumulation [51]. B227 pericarp had a significantly higher content of chlorophyll than that in B214 (Figure 1). These results suggest that *bHLH14* is a strong candidate for the *pc* locus, which may regulate chlorophyll and flavonoid biosynthesis, and thus pericarp coloration in wax gourd. Further work is underway to prove this hypothesis.

## 5. Conclusions

In conclusion, physiological and integrated metabolic and transcriptomic analyses were performed to understand the potential regulatory pathways involved in the fruit color variation in wax gourd. The dark green-colored inbred line B227 contained a higher content of chlorophyll than the yellow-colored inbred line B214. A total of 229 DAMs were identified between the two lines, and flavone C-glycosides were more accumulated in B214. Key genes in the chlorophyll biosynthesis pathway and flavonoid biosynthesis pathway were differentially expressed between the two lines. In addition, *bHLH14* in the previously mapped *pc* locus controlling pericarp color of wax gourd had a higher expression in B227 than in B214. We propose that fruit coloration of the wax gourd pericarp is a complex network, but *bHLH14* probably acts as a key factor in determining chlorophyll and flavonoid synthesis. The results provide valuable information for understanding the complex mechanism of the coloration of wax gourd and its breeding applications.

**Supplementary Materials:** The following supporting information can be downloaded at: <https://www.mdpi.com/article/10.3390/agronomy12092045/s1>, Figure S1: KEGG enrichment analysis of the DEGs and DAMs, which were enriched in the same pathway; Table S1: Differentially accumulated metabolites between mature pericarp of B227 and B214; Table S2: Differentially expressed genes between mature fruit pericarp of B227 and B214; Table S3: KEGG pathway assignment of differentially expressed genes between pericarp of B227 and B214; Table S4: Primer Information of Primers Used in Real-time PCR Validation.

**Author Contributions:** Conceptualization, B.J. and Q.S.; methodology, Q.P.; formal analysis, J.Y., P.S., W.L. and M.W.; resources, B.J., W.L. and D.X.; writing—original draft preparation, J.Y. and P.S.; writing—review and editing, B.J. and J.Y. All authors have read and agreed to the published version of the manuscript.

**Funding:** This research was partially supported by the Key-Area Research and Development Program of Guangdong Province (2020B020220003), the Discipline Team Construction Project of GDAAS (202114TD), the Training Plan for Young and Middle-aged Discipline Leaders of GDAAS (R2020PY-JG003), and the Project of Collaborative Innovation Center of GDAAS (XTXM2002203). The funding agencies played no role in the design of the study, data collection, analysis, and interpretation or writing the manuscript.

**Informed Consent Statement:** Not applicable.

**Data Availability Statement:** The RNA-seq datasets presented in this study can be found at National Center for Biotechnology Information (NCBI) BioProject database under accession number PRJNA863128.

**Conflicts of Interest:** The authors declare no conflict of interest.

## References

1. Chopra, R.N.; Nayar, S.L.; Chopra, K. *Glossary of Indian Medicinal Plants*; Central Institute of Scientific and Industrial Research (CSIR): New Delhi, India, 1956; pp. 35–36.
2. Warriar, P.K.; Nambiar, V.; Ramankutty, C. *Indian Medicinal Plants*; Orient Longman Limited: Kottakkal, India, 1993; p. 261.
3. Koes, R.; Verweij, W.; Quattrocchio, F. Flavonoids: A colorful model for the regulation and evolution of biochemical pathways. *Trends Plant Sci.* **2005**, *10*, 236–242. [[CrossRef](#)] [[PubMed](#)]
4. Lai, B.; Hu, B.; Qin, Y.-H.; Zhao, J.-T.; Wang, H.-C.; Hu, G.-B. Transcriptomic analysis of Litchi chinensis pericarp during maturation with a focus on chlorophyll degradation and flavonoid biosynthesis. *BMC Genom.* **2015**, *16*, 225. [[CrossRef](#)] [[PubMed](#)]
5. Liu, H.; Jiao, J.; Liang, X.; Liu, J.; Meng, H.; Chen, S.; Li, Y.; Cheng, Z. Map-based cloning, identification and characterization of the w gene controlling white immature fruit color in cucumber (*Cucumis sativus* L.). *Theor. Appl. Genet.* **2016**, *129*, 1247–1256. [[CrossRef](#)]
6. Tang, H.-Y.; Dong, X.; Wang, J.-K.; Xia, J.-H.; Xie, F.; Zhang, Y.; Yao, X.; Xu, Y.-J.; Wan, Z.-J. Fine Mapping and Candidate Gene Prediction for White Immature Fruit Skin in Cucumber (*Cucumis sativus* L.). *Int. J. Mol. Sci.* **2018**, *19*, 1493. [[CrossRef](#)]
7. Schaart, J.G.; Dubos, C.; Romero De La Fuente, I.; van Houwelingen, A.M.M.L.; de Vos, R.C.H.; Jonker, H.H.; Xu, W.; Routaboul, J.M.; Lepiniec, L.; Bovy, A.G. Identification and characterization of MYB-bHLH-WD40 regulatory complexes controlling proanthocyanidin biosynthesis in strawberry (*Fragaria × ananassa*) fruits. *New Phytol.* **2013**, *197*, 454–467. [[CrossRef](#)]
8. Petrucci, E.; Braidot, E.; Zancani, M.; Peresson, C.; Bertolini, A.; Patui, S.; Vianello, A. Plant Flavonoids—Biosynthesis, Transport and Involvement in Stress Responses. *Int. J. Mol. Sci.* **2013**, *14*, 14950–14973. [[CrossRef](#)]
9. Takos, A.M.; Jaffé, F.W.; Jacob, S.R.; Bogs, J.; Robinson, S.P.; Walker, A.R. Light-Induced Expression of a MYB Gene Regulates Anthocyanin Biosynthesis in Red Apples. *Plant Physiol.* **2006**, *142*, 1216–1232. [[CrossRef](#)]
10. Zhang, L.; Hu, J.; Han, X.; Li, J.; Gao, Y.; Richards, C.M.; Zhang, C.; Tian, Y.; Liu, G.; Gul, H.; et al. A high-quality apple genome assembly reveals the association of a retrotransposon and red fruit colour. *Nat. Commun.* **2019**, *10*, 1494. [[CrossRef](#)] [[PubMed](#)]
11. Ampomah-Dwamena, C.; Thrimawithana, A.H.; Dejnopratt, S.; Lewis, D.; Espley, R.V.; Allan, A.C. A kiwifruit (*Actinidia deliciosa*) R2R3-MYB transcription factor modulates chlorophyll and carotenoid accumulation. *New Phytol.* **2019**, *221*, 309–325. [[CrossRef](#)]
12. Jin, W.; Wang, H.; Li, M.; Wang, J.; Yang, Y.; Zhang, X.; Yan, G.; Zhang, H.; Liu, J.; Zhang, K. The R2R3 MYB transcription factor PavMYB10.1 involves in anthocyanin biosynthesis and determines fruit skin colour in sweet cherry (*Prunus avium* L.). *Plant Biotechnol. J.* **2016**, *14*, 2120–2133. [[CrossRef](#)] [[PubMed](#)]
13. Yao, G.; Ming, M.; Allan, A.C.; Gu, C.; Li, L.; Wu, X.; Wang, R.; Chang, Y.; Qi, K.; Zhang, S.; et al. Map-based cloning of the pear gene MYB114 identifies an interaction with other transcription factors to coordinately regulate fruit anthocyanin biosynthesis. *Plant J. Cell Mol. Biol.* **2017**, *92*, 437–451. [[CrossRef](#)] [[PubMed](#)]
14. Li, X.; Chen, L.; Hong, M.; Zhang, Y.; Zu, F.; Wen, J.; Yi, B.; Ma, C.; Shen, J.; Tu, J.; et al. A Large Insertion in bHLH Transcription Factor BrTT8 Resulting in Yellow Seed Coat in Brassica rapa. *PLoS ONE* **2012**, *7*, e44145. [[CrossRef](#)] [[PubMed](#)]
15. Ben Zvi, M.M.; Shklarman, E.; Masci, T.; Kalev, H.; Debener, T.; Shafir, S.; Ovadis, M.; Vainstein, A. PAPI transcription factor enhances production of phenylpropanoid and terpenoid scent compounds in rose flowers. *New Phytol.* **2012**, *195*, 335–345. [[CrossRef](#)]
16. Kim, D.-H.; Park, S.; Lee, J.-Y.; Ha, S.-H.; Lim, S.-H. Enhancing Flower Color through Simultaneous Expression of the B-peru and mPAPI Transcription Factors under Control of a Flower-Specific Promoter. *Int. J. Mol. Sci.* **2018**, *19*, 309. [[CrossRef](#)] [[PubMed](#)]
17. Hinchliffe, D.J.; Condon, B.D.; Thyssen, G.; Naoumkina, M.; Madison, C.A.; Reynolds, M.; Delhom, C.D.; Fang, D.D.; Li, P.; McCarty, J. The GhTT2\_A07 gene is linked to the brown colour and natural flame retardancy phenotypes of Lc1 cotton (*Gossypium hirsutum* L.) fibres. *J. Exp. Bot.* **2016**, *67*, 5461–5471. [[CrossRef](#)]
18. Wang, Z.; Cui, Y.; Vainstein, A.; Chen, S.; Ma, H. Regulation of Fig (*Ficus carica* L.) Fruit Color: Metabolomic and Transcriptomic Analyses of the Flavonoid Biosynthetic Pathway. *Front. Plant Sci.* **2017**, *8*, 1990. [[CrossRef](#)] [[PubMed](#)]
19. Lou, Q.; Liu, Y.; Qi, Y.; Jiao, S.; Tian, F.; Jiang, L.; Wang, Y. Transcriptome sequencing and metabolite analysis reveals the role of delphinidin metabolism in flower colour in grape hyacinth. *J. Exp. Bot.* **2014**, *65*, 3157–3164. [[CrossRef](#)]
20. Lv, Y.; Amanullah, S.; Liu, S.; Zhang, C.; Liu, H.; Zhu, Z.; Zhang, X.; Gao, P.; Luan, F. Comparative Transcriptome Analysis Identified Key Pathways and Genes Regulating Differentiated Stigma Color in Melon (*Cucumis melo* L.). *Int. J. Mol. Sci.* **2022**, *23*, 6721. [[CrossRef](#)]
21. Zhao, G.; Wang, M.; Luo, C.; Li, J.; Gong, H.; Zheng, X.; Liu, X.; Luo, J.; Wu, H. Metabolome and Transcriptome Analyses of Cucurbitacin Biosynthesis in Luffa (*Luffa acutangula*). *Front. Plant Sci.* **2022**, *13*, 886870. [[CrossRef](#)]
22. Rhee, S.J.; Seo, M.; Jang, Y.J.; Cho, S.; Lee, G.P. Transcriptome profiling of differentially expressed genes in floral buds and flowers of male sterile and fertile lines in watermelon. *BMC Genom.* **2015**, *16*, 914. [[CrossRef](#)]
23. Rhee, S.-J.; Jang, Y.J.; Park, J.-Y.; Ryu, J.; Lee, G.P. Virus-induced gene silencing for *in planta* validation of gene function in cucurbits. *Plant Physiol.* **2022**, kiac363. [[CrossRef](#)] [[PubMed](#)]
24. Jiang, B.; Liu, W.; Xie, D.; Peng, Q.; He, X.; Lin, Y.; Liang, Z. High-density genetic map construction and gene mapping of pericarp color in wax gourd using specific-locus amplified fragment (SLAF) sequencing. *BMC Genom.* **2015**, *16*, 1035. [[CrossRef](#)] [[PubMed](#)]
25. Lichtenthaler, H.K.; Wellburn, A.R. Determinations of total carotenoids and chlorophylls a and b of leaf extracts in different solvents. *Analysis* **1983**, *11*, 591–592. [[CrossRef](#)]

26. Chen, W.; Gong, L.; Guo, Z.; Wang, W.; Zhang, H.; Liu, X.; Yu, S.; Xiong, L.; Luo, J. A Novel Integrated Method for Large-Scale Detection, Identification, and Quantification of Widely Targeted Metabolites: Application in the Study of Rice Metabolomics. *Mol. Plant* **2013**, *6*, 1769–1780. [[CrossRef](#)]
27. Fraga, C.G.; Clowers, B.H.; Moore, R.J.; Zink, E.M. Signature-Discovery Approach for Sample Matching of a Nerve-Agent Precursor Using Liquid Chromatography-Mass Spectrometry, XCMS, and Chemometrics. *Anal. Chem.* **2010**, *82*, 4165–4173. [[CrossRef](#)]
28. Wang, S.; Tu, H.; Wan, J.; Chen, W.; Liu, X.; Luo, J.; Xu, J.; Zhang, H. Spatio-temporal distribution and natural variation of metabolites in citrus fruits. *Food Chem.* **2016**, *199*, 8–17. [[CrossRef](#)]
29. Wang, L.; Feng, Z.; Wang, X.; Wang, X.; Zhang, X. DEGseq: An R package for identifying differentially expressed genes from RNA-seq data. *Bioinformatics* **2010**, *26*, 136–138. [[CrossRef](#)]
30. Mortazavi, A.; Williams, B.A.; McCue, K.; Schaeffer, L.; Wold, B. Mapping and quantifying mammalian transcriptomes by RNA-Seq. *Nat. Methods* **2008**, *5*, 621–628. [[CrossRef](#)]
31. Götz, S.; Garcia-Gomez, J.M.; Terol, J.; Williams, T.D.; Nagaraj, S.H.; Nueda, M.J.; Robles, M.; Talón, M.; Dopazo, J.; Conesa, A. High-throughput functional annotation and data mining with the Blast2GO suite. *Nucleic Acids Res.* **2008**, *36*, 3420–3435. [[CrossRef](#)]
32. Bo, K.; Wei, S.; Wang, W.; Miao, H.; Dong, S.; Zhang, S.; Gu, X. QTL mapping and genome-wide association study reveal two novel loci associated with green flesh color in cucumber. *BMC Plant Biol.* **2019**, *19*, 243. [[CrossRef](#)]
33. Li, Y.; Wen, C.; Weng, Y. Fine mapping of the pleiotropic locus B for black spine and orange mature fruit color in cucumber identifies a 50 kb region containing a R2R3-MYB transcription factor. *Theor. Appl. Genet.* **2013**, *126*, 2187–2196. [[CrossRef](#)] [[PubMed](#)]
34. Che, G.; Zhang, X. Molecular basis of cucumber fruit domestication. *Curr. Opin. Plant Biol.* **2019**, *47*, 38–46. [[CrossRef](#)] [[PubMed](#)]
35. Guo, S.; Zhao, S.; Sun, H.; Wang, X.; Wu, S.; Lin, T.; Ren, Y.; Gao, L.; Deng, Y.; Zhang, J.; et al. Resequencing of 414 cultivated and wild watermelon accessions identifies selection for fruit quality traits. *Nat. Genet.* **2019**, *51*, 1616–1623. [[CrossRef](#)] [[PubMed](#)]
36. Ohmiya, A.; Sasaki, K.; Nashima, K.; Oda-Yamamizo, C.; Hirashima, M.; Sumitomo, K. Transcriptome analysis in petals and leaves of chrysanthemums with different chlorophyll levels. *BMC Plant Biol.* **2017**, *17*, 202. [[CrossRef](#)] [[PubMed](#)]
37. Wu, H.; Shi, N.; An, X.; Liu, C.; Fu, H.; Cao, L.; Feng, Y.; Sun, D.; Zhang, L. Candidate Genes for Yellow Leaf Color in Common Wheat (*Triticum aestivum* L.) and Major Related Metabolic Pathways according to Transcriptome Profiling. *Int. J. Mol. Sci.* **2018**, *19*, 1594. [[CrossRef](#)]
38. Hao, N.; Du, Y.; Li, H.; Wang, C.; Wang, C.; Gong, S.; Zhou, S.; Wu, T. CsMYB36 is involved in the formation of yellow green peel in cucumber (*Cucumis sativus* L.). *Theor. Appl. Genet.* **2018**, *131*, 1659–1669. [[CrossRef](#)]
39. Wu, Q.; Tian, J.; Li, P.-C.; Zhang, H.-J.; Feng, C.-Y.; Li, S.-S.; Yin, D.-D.; Xu, W.-Z.; Wang, L.-S. Relationship between the flavonoid composition and flower colour variation in *Victoria*. *Plant Biol.* **2018**, *20*, 674–681. [[CrossRef](#)]
40. Gao, J.; Ren, R.; Wei, Y.; Jin, J.; Ahmad, S.; Lu, C.; Wu, J.; Zheng, C.; Yang, F.; Zhu, G. Comparative Metabolomic Analysis Reveals Distinct Flavonoid Biosynthesis Regulation for Leaf Color Development of *Cymbidium sinense* ‘Red Sun’. *Int. J. Mol. Sci.* **2020**, *21*, 1869. [[CrossRef](#)]
41. Liao, J.; Zang, J.; Yuan, F.; Liu, S.; Zhang, Y.; Li, H.; Piao, Z.; Li, H. Identification and analysis of anthocyanin components in fruit color variation in *Schisandra chinensis*. *J. Sci. Food Agric.* **2016**, *96*, 3213–3219. [[CrossRef](#)]
42. Zhang, A.; Zheng, J.; Chen, X.; Shi, X.; Wang, H.; Fu, Q. Comprehensive Analysis of Transcriptome and Metabolome Reveals the Flavonoid Metabolic Pathway Is Associated with Fruit Peel Coloration of Melon. *Molecules* **2021**, *26*, 2830. [[CrossRef](#)]
43. Han, S.J.; Ryu, S.N.; Trinh, H.T.; Joh, E.H.; Jang, S.Y.; Han, M.J.; Kim, D.H. Metabolism of Cyanidin-3-O-Beta-D-Glucoside Isolated from Black Colored Rice and Its Antiscratching Behavioral Effect in Mice. *J. Food Sci.* **2019**, *74*, H253–H258. [[CrossRef](#)] [[PubMed](#)]
44. Morita, Y.; Hoshino, A.; Kikuchi, Y.; Okuhara, H.; Ono, E.; Tanaka, Y.; Fukui, Y.; Saito, N.; Nitasaka, E.; Noguchi, H.; et al. Japanese morning glory dusky mutants displaying reddish-brown or purplish-gray flowers are deficient in a novel glycosylation enzyme for anthocyanin biosynthesis, UDP-glucose: Anthocyanidin 3-O-glucoside-2''-O-glucosyltransferase, due to 4-bp insertions in the Gene. *Plant J.* **2005**, *42*, 353–363. [[CrossRef](#)] [[PubMed](#)]
45. Han, Y.; Vimolmangkang, S.; Soria-Guerra, R.E.; Rosales-Mendoza, S.; Zheng, D.; Lygin, A.V.; Korban, S.S. Ectopic Expression of Apple *F3'H* Genes Contributes to Anthocyanin Accumulation in the *Arabidopsis* *tt7* Mutant Grown Under Nitrogen Stress. *Plant Physiol.* **2010**, *153*, 806–820. [[CrossRef](#)] [[PubMed](#)]
46. He, H.; Ke, H.; Keting, H.; Qiaoyan, X.; Silan, D. Flower Colour Modification of Chrysanthemum by Suppression of *F3'H* and Overexpression of the Exogenous *Senecio cruentus* *F3'5'H* Gene. *PLoS ONE* **2013**, *8*, e74395. [[CrossRef](#)]
47. Nishizaki, Y.; Sasaki, N.; Yasunaga, M.; Miyahara, T.; Okamoto, E.; Okamoto, M.; Hirose, Y.; Ozeki, Y. Identification of the glucosyltransferase gene that supplies the p-hydroxybenzoyl-glucose for 7-polyacylation of anthocyanin in delphinium. *J. Exp. Bot.* **2014**, *65*, 2495–2506. [[CrossRef](#)]
48. Zhang, Y.-L.; Fang, Z.-Z.; Ye, X.-F.; Pan, S.-L. Identification of candidate genes involved in anthocyanin accumulation in the peel of jaborcaba (*Myrciaria cauliflora*) fruits by transcriptomic analysis. *Gene* **2018**, *676*, 202–213. [[CrossRef](#)]
49. Nakayama, M.; Koshioka, M.; Kondo, T.; Imizu, K. Flavone C-Glucosides Responsible for Yellow Pigmentation Induced by Low Temperature in Bracts of *Zantedeschia aethiopica*. *Nat. Prod. Commun.* **2015**, *10*, 425–427. [[CrossRef](#)]

50. Qi, T.; Wang, J.; Huang, H.; Liu, B.; Gao, H.; Liu, Y.; Song, S.; Xie, D. Regulation of Jasmonate-Induced Leaf Senescence by Antagonism between bHLH Subgroup IIIe and IIIId Factors in Arabidopsis. *Plant Cell* **2015**, *27*, 1634–1649. [[CrossRef](#)]
51. Song, S.; Qi, T.; Fan, M.; Zhang, X.; Gao, H.; Huang, H.; Wu, D.; Guo, H.; Xie, D. The bHLH Subgroup IIIId Factors Negatively Regulate Jasmonate-Mediated Plant Defense and Development. *PLoS Genet.* **2013**, *9*, e1003653. [[CrossRef](#)]